Optical Properties of Single-Walled 4 Å Carbon Nanotubes

WanZhen Liang,† Satoshi Yokojima,† Man-Fai Ng,† GuanHua Chen,*,† and Guozhong He‡

Contribution from the Department of Chemistry, The University of Hong Kong, Pokfulam Road, Hong Kong, China, and Dalian Institute of Chemical Physics, Chinese Academy of Sciences, Dalian, China

Received April 18, 2001

Abstract: Optical properties of a series of finite sized hydrogenated carbon nanotubes with the smallest diameter of 4 Å are studied systematically. Their absorption spectra are calculated with the localized-density-matrix method. The semiempirical MNDO parametric method 3 (PM3) Hamiltonian is employed. The finite optical gaps are predicted for the infinite long single-walled carbon nanotubes. Strong anisotropy characteristics of the dynamic polarizabilities are found for these tubes. The calculated results are in good agreement with the recent experimental findings. Further the compositions of the dipole-induced excitations are examined by projecting the corresponding density matrices onto the Hartree−Fock molecular orbital representation. Unlike the larger diameter carbon nanotubes whose absorption spectra are insensitive to the tube chiralities, the absorption spectra of 4 Å single-walled carbon nanotubes depend very much on their chiralities. The chirality of the single-walled 4 Å carbon nanotubes synthesized in the channels of the porous zeolites is thus determined to be (5,0) by comparing the calculated and measured absorption spectra.

1. Introduction

Because of their exciting physical properties and potential applications, carbon nanotubes (CNTs) have become the major subject of numerous experimental and theoretical investigation since the initial finding by Iijima in 1991[1] and the subsequent report of the synthesis of large quantities of CNTs by Ebbesen et al. in 1992.[2] Both open-ended and capped CNTs have been observed by high-resolution transmission electron microscope (TEM)[1,3] and STM[4] techniques. The excitement of this discovery was amplified when several theoretical studies revealed that CNTs would be either metallic or semiconducting, depending on their chiralities.[5−8] These theoretical predictions have been confirmed in STM[9−12] and EELS[13−15] experiments. The optical properties of CNTs have been measured.[15−19] The CNTs in these experiments are either multiwalled CNTs or an ensemble of single-walled CNTs (SWNTs). The anisotropic properties of carbon nanotubes have been investigated experimentally by de Heer and his colleagues.[19] The dielectric function ϵ was found highly anisotropic being much larger when the electric field is aligned along the tube axis than when it is aligned perpendicular to the tube axis. Theoretical calculations have been carried out to examine the electronic structures and optical properties of SWNTs.[5−8,20−25] Tight-binding[5−8] and density functional theory (DFT) calculations[20,21] conclude that an (m,n) SWNT is a conductor if $m - n = 3I$ (I is an integer) and a semiconductor if $m - n \neq 3I$.[5−8] Moreover, the detailed plane-wave ab initio pseudopotential local density approximation (LDA) calculations[26] predicted that all small diameter tubes are conductors regardless of their chiralities. A series of SWNTs have been investigated systematically by the localized-density-matrix (LDM) method.[27−30] Two types of dipole-induced excitations have been identified, the low-energy (ω < 1.0 eV) excitations

* Author to whom correspondence should be addressed.
† The University of Hong Kong.
‡ Chinese Academy of Sciences.

(1) Iijima, S. *Nature* **1991**, *354*, 56.
(2) (a) Ebbesen, T. W.; Ajayan, P. M. *Nature* **1992**, *358*, 220. (b) Ebbesen, T. W.; Hiura, H.; Fujita, J.; Ochiai, Y.; Matsui, S.; Tanigaki, K. *Chem. Phys. Lett.* **1993**, *209*, 83.
(3) Iijima, S. *Mater. Sci. Eng. B* **1993**, *19*, 172.
(4) Sattler, K. *Carbon* **1995**, *33*, 915.
(5) Hamada, N.; Sawada, S.; Oshiyama, A. *Phys. Rev. Lett.* **1992**, *68*, 1579.
(6) Dresselhaus, M. S.; Dresselhaus, G.; Eklund, P. C. *Science of Fullerenes and Carbon Nanotubes*; Academic Press: San Diego, CA, 1996.
(7) (a) Saito, R.; Fujita, M.; Dresselhaus, G.; Dresselhaus, M. S. *Appl. Phys. Lett.* **1992**, *60*, 2204. (b) Saito, R.; Fujita, M.; Dresselhaus, G.; Dresselhaus, M. S. *Phys. Rev. B* **1992**, *46*, 1804.
(8) Saito, R.; Dresselhaus, G.; Dresselhaus, M. S. *Physical Properties of Carbon Nanotubes*; Imperial College Press: London, 1998.
(9) Zhang, Z.; Lieber, C. M. *Appl. Phys. Lett.* **1993**, *62*, 2792.
(10) Olk, C. H.; Heremans, J. P. *J. Mater. Res.* **1994**, *9*, 259.
(11) Wildöer, J. W. G.; Venema, L. C.; Rinzler, A. G.; Smalley, R. E.; Dekker, C. *Nature* **1998**, *391*, 59.
(12) Odom, T. W.; Huang, J.-L.; Kim P.; Lieber, C. M. *Nature* **1998**, *391*, 62.
(13) Dravid, V. P.; Lin, X.; Wang, Y.; Wang, X. K.; Yee, A.; Ketterson, J. B.; Chang, R. P. H. *Science* **1993**, *259*, 1601.
(14) Ajayan, P. M.; Iijima, S.; Ichihashi, T. *Phys. Rev. B* **1993**, *47*, 6859.
(15) Pichler, T.; Knupfer, M.; Golden, M. S.; Fink, J.; Rinzler, A.; Smalley, R. E. *Phys. Rev. Lett.* **1998**, *80*, 4729.
(16) Liu, X.; Si, J.; Chang, B.; Xu, G.; Yang, Q.; Pan, Z.; Xie, S.; Ye, P.; Fan, J.; Wan, M. *Appl. Phys. Lett.* **1999**, *74*, 164.
(17) Chen, J.; Hamon, M. A.; Hu, H.; Chen, Y.; Rao, A. M.; Eklund, P. C.; Haddon, R. C. *Science* **1998**, *282*, 95.
(18) Hamon, M. A.; Chen, J.; Hu, H.; Chen, Y.; Itkis, M. E.; Rao, A. M.; Eklund, P. C.; Haddon, R. C. *Adv. Mater.* **1999**, *11*, 834.
(19) de Heer, W. A.; Bacsa, W. S.; Châtelain, A.; Gerfin, T.; Humphrey-Baker, R.; Forro, L.; Ugarte, D. *Science* **1995**, *268*, 845.
(20) Rubio, A. *Appl. Phys. A* **1999**, *68*, 275.
(21) Rubio, A.; Sánchez-Portal, D.; Artacho, E.; Ordejón, P.; Soler, J. M. *Phys. Rev. Lett.* **1999**, *82*, 3520.
(22) Wan, X.; Dong, J.; Xing, D. Y. *Phys. Rev. B* **1998**, *58*, 6756.
(23) Ma, J.; Yuan, R.-K. *Phys. Rev. B* **1998**, *57*, 9343.
(24) Ando, T. *J. Phys. Soc. Jpn.* **1997**, *66*, 1066.
(25) (a) Jiang, J.; Dong J.; Wan, X.; Xing, D. Y. *J. Phys. B* **1998**, *31*, 3079. (b) Jiang, J.; Dong J.; Xing, D. Y. *Phys. Rev. B* **1999**, *59*, 9838.
(26) Blase, X.; Benedict, L. X.; Shirley, E. L.; Louie, S. G. *Phys. Rev. Lett.* **1994**, *72*, 1878.
(27) Yokojima, S.; Chen, G. H. *Phys. Rev. B* **1999**, *59*, 7259.
(28) Yokojima, S.; Chen, G. H. *Chem. Phys. Lett.* **1998**, *292*, 379.

10.1021/ja0160445 CCC: $20.00
Published on Web 09/18/2001

and high-energy ($\omega > 1.0$ eV) excitations. The low-energy excitations are the electron−hole pairs confined to the two ends of open-ended CNTs, and the higher energy excitations locate mainly along the tube.[30] These SWNTs whose optical properties have been calculated are mainly armchair and zigzag tubes, and their diameters are much larger than 4 Å. It was found that the absorption spectra of large diameter carbon nanotubes are determined mainly by their diameters and that the chiralities have little effect.[30]

As early as 1992, Sawada and Hamada[31] predicted the existence of extremely thin tubules, for instance, 4 Å CNTs. They calculated the cohesive energies of the CNTs using the Tersoff's empirical potential for carbon[32] and showed that not only large diameter tubules but also small diameter tubules are energetically more favorable than the graphite sheets of the same width. They thus suggested that the 4 Å CNTs may exist. Recently both multiwalled and single-walled 4 Å CNTs have been synthesized respectively by the mass-selected carbon ion beam deposition (MSIBD) method[33,34] and by the pyrolysis of tripropylamine molecules in the channels of porous zeolite $AlPO_4$-5 (AFI) single crystals.[35] The single-walled 4 Å CNTs are the best examples of one-dimensional quantum wires. The 4 Å CNTs have three possible structures: the chiral (4,2) CNT, the zigzag (5,0) CNT, or the armchair (3,3) CNT. Their diameters are 4.2, 3.9, and 4.1 Å, respectively. It has been argued that the 4 Å CNTs may be either (3,3) or (5,0) because they fit well with the half fullerene C_{20} cap.[33] The corresponding electronic structures and optical properties have been measured experimentally.[36] Three major absorption peaks at 1.35, 2.15, and 3.10 eV are identified in the absorption spectra when the electric field is parallel to the tubes. When the external field is perpendicular to the tube axis, the CNTs are almost transparent. A very weak absorption peak is observed with its energy slightly lower than 1.35 eV.[36]

In this paper we report the calculations of the optical properties of the SWNTs (4,2), (3,3), and (5,0) using the LDM-PM3 method.[30] By comparing the calculated and measured absorption spectra, we determine the chirality of the 4 Å SWNT synthesized in the channels of the porous zeolite.[36] The anisotropy of the absorption spectra is investigated by calculating the dynamic polarizabilities for different light polarizations. The nature of the dipole-induced excitations is examined by projecting the corresponding reduced single-electron density matrices onto the Hartree−Fock molecular orbital (HFMO) representation. Possible dipole-induced transitions among the molecular orbitals are determined for (3,3) and (5,0) SWNTs. The paper is organized as follows: Section 2 contains a brief description of the LDM-PM3 methods. The calculated optical absorption spectra of (4,2), (3,3) and (5,0) are presented in Section 3. Detailed analysis of the dipole-induced excitations in the HFMO representation is reported. The symmetry of each molecular orbital (MO) is given, and possible dipole-induced optical transitions are identified among them. Finally the conclusion is given in Section 4.

2. The LDM-PM3 Method

The linear polarization tensor α is defined as[37,38]

$$\alpha_{ij} = \left.\frac{d\mathbf{P}_i(\omega)}{d\mathbf{E}_j(\omega)}\right|_{\mathbf{E}=0} \tag{1}$$

Here $\boldsymbol{P}(\omega)$ is the electric polarization vector, $\boldsymbol{E}(\omega)$ is the external electric field, and i or j is the index representing x, y, or z components of a vector. The electric polarization is a physical observable and is defined by the expectation values of microscopic polarization operator $\hat{\mathscr{P}}$

$$\mathbf{P}(\mathbf{r},t) = \mathrm{Tr}[\hat{\mathscr{P}}(\mathbf{r})\,\rho(t)] \tag{2}$$

where $\rho(t)$ is the reduced single-electron density matrix that can be obtained by solving the time-dependent Hartree−Fock (TDHF) equation of motion[39]

$$\left(i\hbar\frac{d}{dt} + \gamma\right)\rho(t) = [h,\rho(t)] \tag{3}$$

Here h is the Fock operator of the system and γ is the phenomenological dephasing constant. The PM3 Hamiltonian[40] in the presence of an external field $\mathbf{E}$ is described as follows,

$$H = H_e + H_{ee} + H_{ext} = \sum_{ab}\sum_{mn} H_{ab}^{mn} c_{am}^{\dagger} c_{bn} + \frac{1}{2}\sum_{ab}\sum_{mnij} V_{ab}^{mn,ij} c_{an}^{\dagger} c_{bi}^{\dagger} c_{bj} c_{am} - \mathbf{E}\cdot\sum_{mn}\mathbf{P}_{ab}^{mn} c_{am}^{\dagger} c_{bn} \tag{4}$$

where $c_{am}^{\dagger}$ (c_{bn}) is the creation (annihilation) operator for an electron at a localized atomic spin spatial orbital m (n) on atom a (b). One-electron integral H_{ab}^{mn} may be expressed as

$$H_{ab}^{mn} = \left\langle \chi_a^m \middle| -\frac{1}{2}\nabla_{\mathbf{r}}^2 + \boldsymbol{U}(\mathbf{r}) \middle| \chi_b^n \right\rangle \tag{5}$$

where χ_a^m (χ_b^n) is the m (n)-th atomic orbital on atom a (b) and $U(\mathbf{r})$ is the one-electron potential. H_{ee} is the two-electron part of the Hamiltonian that represents the effective electron−electron Coulomb interaction. The PM3 model utilizes the neglect of differential overlap for atomic orbitals on different atoms, i.e., all the two-electron integrals are set to zero except that when the orbitals m and n belong to the same atom a and i and j belong to atom b. $V_{ab}^{mn,ij}$ is expressed as

$$V_{ab}^{mn,ij} = \langle \chi_a^n(1)\chi_b^i(2)|V(r_{12})|\chi_a^m(1)\chi_b^j(2)\rangle \tag{6}$$

H_{ext} is the interaction between the valence electrons and an external electric field $\mathbf{E}(t)$, and $\hat{\mathbf{P}}$ is the molecular dipole moment operator. $\mathbf{P}_{ab}^{mn}$ is calculated by $\langle \chi_a^m|\hat{\mathbf{P}}|\chi_b^n\rangle$, neglecting the diatomic overlap. Considering the linear response only, ρ may be expressed as $\rho = \rho^{(0)} + \delta\rho$, where $\rho^{(0)}$ is the Hartree−Fock ground-state reduced density matrix when $\mathbf{E}(t) = 0$ and $\delta\rho$ is the induced density matrix in $\mathbf{E}(t)$. Similarly, Fock matrix h may be decomposed as $h = h^{(0)} + \delta h$ where $h^{(0)}$ is the Fock matrix when $\mathbf{E}(t) = 0$ with

(29) Liang, W. Z.; Yokojima, S.; Zhou, D. H.; Chen, G. H. *J. Phys. Chem. A* **2000**, *104*, 2445.
(30) Liang, W. Z.; Wang, X. J.; Yokojima, S.; Chen, G. H. *J. Am. Chem. Soc.* **2000**, *122*, 11129.
(31) Sawada, S.; Hamada, N. *Solid State Commun.* **1992**, *83*, 917.
(32) Tersoff, J. *Phys. Rev. Lett.* **1988**, *61*, 2879.
(33) Qin, L.-C.; Zhao, X.; Hirahara, K.; Miyamoto, Y.; Ando, Y.; Iijima, S. *Nature* **2000**, *408*, 50.
(34) Peng, H. Y.; Wang, N.; Zheng, Y. F.; Lifshitz, Y.; Kulik, J.; Zhang, R. Q.; Lee, C. S.; Lee, S. T. *Appl. Phys. Lett.* **2000**, *77*, 2831.
(35) Wang, N.; Tang, Z. K.; Li, G. D.; Chen, J. S. *Nature* **2000**, *408*, 50.
(36) Tang, Z. K. Private communication.
(37) Mukamel, S. *Principle of Nonlinear Optical Spectroscopy*; Oxford University Press: New York, 1995.
(38) Lin, S. H.; Alden, R.; Islampour, R.; Ma, H.; Villaeys, A. A. *Density Matrix Method and Femtosecond Processes*; World Scientific: Singapore, 1991.
(39) Ring, P.; Schuck, P. *The Nuclear Many-Body Problem*; Springer: New York, 1980.
(40) Stewart, J. J. P. *J. Comput. Chem.* **1989**, *10*, 209.

$$h_{ab}^{(0)mn} = H_{ab}^{mn} + 2\delta_{ab}\sum_{c}\sum_{ij\in c} V_{ac}^{mn,ij}\rho_{cc}^{(0)ij} - \sum_{i\in a}\sum_{j\in b} V_{ab}^{mi,jn}\rho_{ab}^{(0)ij} \quad (7)$$

And similarly, the induced Fock matrix may be expressed as follows,

$$\delta h_{ab}^{mn} = 2\delta_{ab}\sum_{c}\sum_{ij\in c} V_{ac}^{mn,ij}\delta\rho_{cc}^{ij} - \sum_{i\in a}\sum_{j\in b} V_{ab}^{mi,jn}\delta\rho_{ab}^{ij} \quad (8)$$

Thus we have the following equation for the linear response.

$$\left(i\hbar\frac{\mathrm{d}}{\mathrm{d}t} + \gamma\right)\delta\rho(t) = [h^{(0)},\delta\rho(t)] + [\delta h(t),\rho^{(0)}] - \mathbf{E}(t)\cdot[\boldsymbol{P},\rho^{(0)}] \quad (9)$$

The following approximations are employed to achieve the linear-scaling calculation for the excited-state properties:[27−29]

$$\rho_{ab}^{(0)mn} = 0 \text{ if } r_{ab} > l_0$$

$$\delta\rho_{ab}^{mn} = 0 \text{ if } r_{ab} > l_1$$

where r_{ab} are the distances between two atoms *a* and *b*. The details of the LDM-PM3 method can be found in ref 30.

3. Results

Before presenting our results on 4 Å SWNTs, we discuss the absorption spectra of two larger diameter SWNTs for reference. The computed optical absorption spectra of two SWNTs, (9,0) (C_{294}) and (5,5) (C_{290}), are shown in Figure 1. Both SWNTs are capped by a bisected C_{60} molecule at their equators. Geometries are optimized by PM3,[40] and the LDM-PM3 method is employed for the absorption spectra. Solid lines are for (9,0) and dashed lines are for (5,5). In Figure 1a the external field **E** is along tube axis while it is the **E** ⊥ tube in Figure 1b. The diameters of (9,0) and (5,5) are 6.9 and 7.1 Å, respectively. In other words, (9,0) and (5,5) are of the similar diameters. Clearly their absorption spectra are quite similar as well. This supports our earlier conclusion that the chirality of a larger diameter SWNT has little effect on its optical absorption spectrum.[30] Now we examine the optical properties of 4 Å SWNTs.

3.1 Polarization-Dependent Optical Absorption Spectra of 4 Å SWNTs. In our calculations the two ends of SWNTs are terminated with hydrogen atoms. The ideal structures are employed, i.e., the SWNTs are constructed by rolling graphite segments along the tube axis with the C−C bond length set to 1.42 Å except that the structures of (4,2) SWNTs are optimized by the PM3 calculations. For a neutral (5,0) CNT, its electrons cannot fill the closed-shell structure. The unpaired electrons result in a net dipole moment that prevents the converge of the self-consistent field (SCF) calculation.[41] Four extra electrons are added to the (5,0) CNT, upon which the self-consistent computation converges and a set of MOs are obtained. It is expected that the extra four electrons have little effect on the optical response when the number of carbon atom reaches 200 or more. Figures 2−4 show the calculated absorption spectra of different (4,2), (3,3), and (5,0) SWNTs. Each unit cell of (4,2), (3,3), and (5,0) CNTs has 56, 12, and 20 carbon atoms, respectively. All solid lines are the absorption spectra corresponding to the electric field **E** aligned along the tube axis (i.e. **E** || tube) while the dashed lines correspond to **E** perpendicular to the tube (i.e. **E** ⊥ tube). The calculated absorption spectra of

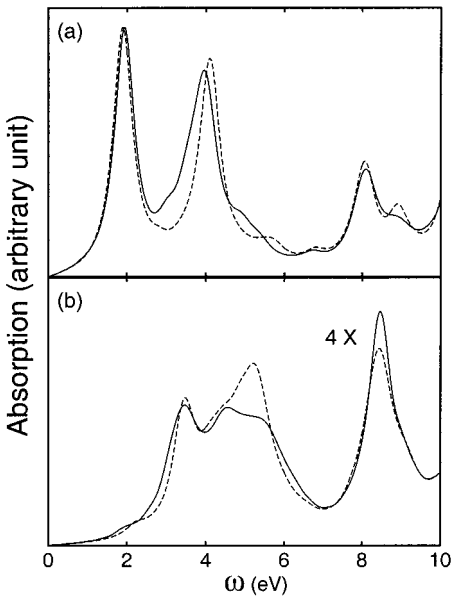

Figure 1. The calculated absorption spectra of capped (9,0) C_{294} (solid line) and (5,5) C_{290} (dashed line) SWNTs. The external field **E** is (a) along the tube axis (**E** || tube) and (b) perpendicular (**E** ⊥ tube) to the tube axis. The absorption spectra in part b are magnified four times. The dephasing parameter $\gamma = 0.3$ eV.

(4,2), (5,0), and (3,3) CNTs are quite different despite the fact that their diameters are almost the same. This differs from our previous calculated results on larger diameter CNTs which showed the absorption spectra are insensitive to the chiralities of CNTs when the tube lengths are long enough. In the case of the **E** || tube, the optical spectra of the three SWNTs depend very much on the tube lengths. As the number of carbon atoms increases, the absorption spectra of the open-ended chiral (4,2) tubes change drastically, especially when the tube lengths are relatively short. The overall spectra red shift and the relative amplitude in the low-energy range ($\omega < 1.0$ eV) reduces as the number of carbon atoms *N* increases. When the (4,2) SWNTs have 200 or more carbon atoms these peaks disappear as compared to the others (see Figure 2). The open-ended (3,3) and (5,0) SWNTs have a different response to the external field as compared to the (4,2) SWNTs. In the low-energy range ($\omega < 1$ eV), no peaks are observed even for very short tubes (see Figures 3 and 4). The two ends play an important role in the optical response for some short tubes, for instance, the (4,2) CNTs. Their influence recedes as the length increases. The optical behavior of the long tubes is affected little by two ends, which is consistent with the experimental observation.[17,18]

Two absorption peaks are found at 1.60 and 2.9 eV for (4,2) $C_{332}H_{12}$ and three peaks at 1.16, 1.66, and 2.60 eV for (5,0) $C_{300}H_{10}$. The (3,3) SWNT has one distinctive strong absorption peak in the low-energy range for $N > 200$. It red shifts when the tube length increases and saturates at 0.61 eV as $N \rightarrow \infty$ (see Figure 5b). Similar red shifts of absorption spectra are observed for (4,2) and (5,0) SWNTs. These red shifts are due to the collective character of the excitation in terms of the single electron−hole excitation picture.[39] Since π electrons delocalize more than σ electrons, the red shifts are prominent for $\omega < 4$ eV because the corresponding excitations are mainly $\pi-\pi^*$ transition. Note that the spectral profiles do not vary much after *N* reaches 200 or more. Therefore, $C_{332}H_{12}$, $C_{420}H_{12}$, and $C_{300}H_{10}$ are used to simulate respectively the infinite long (4,2), (3,3), and (5,0) SWNTs. Given the fact that the absorption spectra are very different for (4,2), (3,3), and (5,0), we conclude that for small-diameter SWNTs the optical response depends on the

(41) Bulusheva, L. G.; Okotrub, A. V.; Romanov, D. A.; Tomanek, D. *J. Phys. Chem. A* **1998**, *102*, 975.

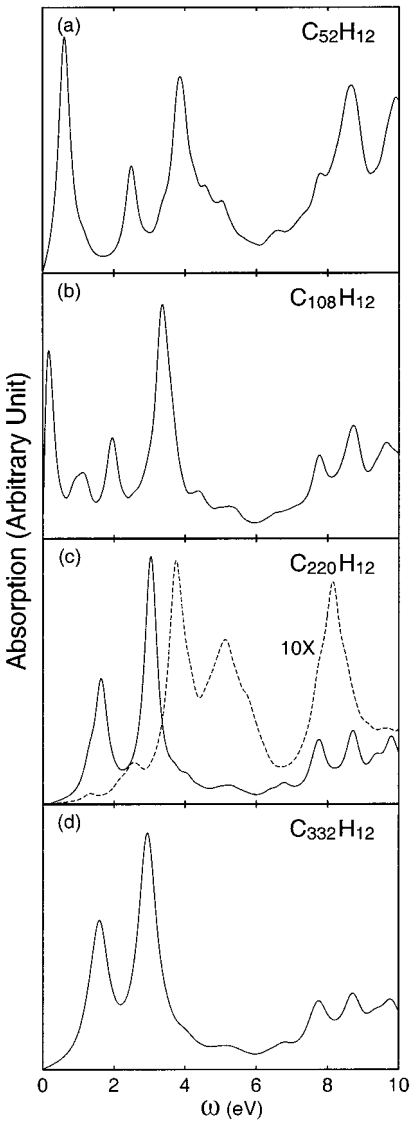

Figure 2. The calculated absorption spectra of (4,2) SWNTs with dephasing parameter $\gamma = 0.2$ (a−c) and 0.3 eV (d). The external field **E** is along the tube axis except for the dashed line in part c, which is the result for the **E** ⊥ tube. The dashed lines are magnified 10 times.

chirality of the tube, besides the diameter and the tube length. Therefore, the observed absorption spectra may be used to determine the structures of 4 Å SWNTs.

To investigate the anisotropy characters of (3,3), (5,0), and (4,2) SWNTs, we calculate their absorption spectra by aligning the external field **E** perpendicular to the tube axis (**E** ⊥ tube). The resulting absorption spectra are shown in dashed lines in Figures 2c, 3a,b, and 4a,c. The strong anisotropy is observed for all three SWNTs. The absorption intensities are much less for the **E** ⊥ tube as compared to the **E** || tube. The anisotropy increases as the tube length increases. This is consistent with the experimental observation[36] that the 4 Å SWNTs are opaque for the **E** || tube but almost transparent for the **E** ⊥ tube. The lowest absorption peak red shifts when the light polarization varies from the parallel direction of the tube to the perpendicular direction.[36] Our calculations show the same phenomenon for (4,2) and (5,0) but not for (3,3). For (4,2) $C_{220}H_{12}$ and (5,0) $C_{300}H_{10}$, their respective optical gaps are 1.33 and 0.70 eV for the **E** ⊥ tube while they are 1.64 and 1.16 eV for the **E** || tube. For (3,3) CNTs, the optical gap is larger for the **E** ⊥ tube than for the **E** || tube.

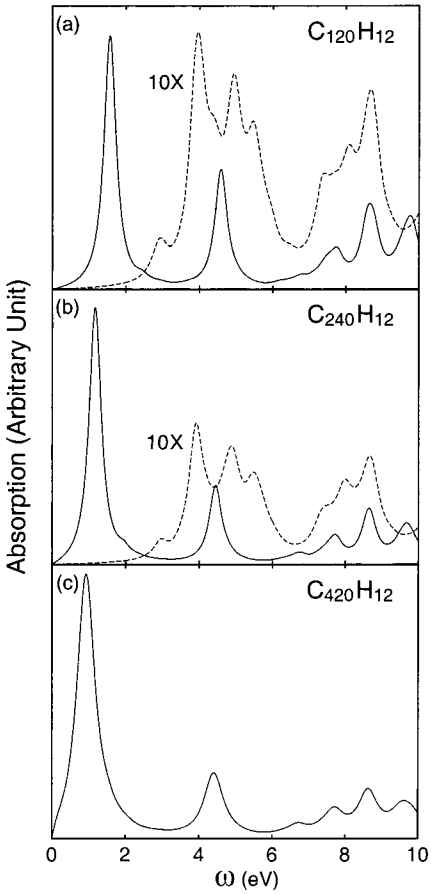

Figure 3. The calculated absorption spectra of (3,3) SWNTs with dephasing parameter $\gamma = 0.2$ (a, b) and 0.3 eV (c). The solid lines are the results for the **E** || tube and the dashed lines for the **E** ⊥ tube. The dashed lines are magnified 10 times.

We plot the optical gaps of the open-ended tubes (4,2), (3,3), and (5,0) versus $1/N$ for the **E** || tube in Figure 5, parts a, b, and c, respectively. The dashed lines are the linear fits. Clearly the gaps depend linearly on $1/N$. The optical gaps of (4,2), (3,3), and (5,0) are respectively 1.5, 0.61, and 0.90 eV as the tubes become infinitely long. In ref 30 we reported the similar findings that the long (6,0), (9,0), (5,5), (8,8), and (10,10) SWNTs have finite optical gaps.

The concept of pyramidalization angle is developed to extend the definition of the π orbital to a nonplanar molecule.[42] To examine the effect of rehybridization of the σ and π electrons on to the optical gap, we calculate the pyramidalization angle[42] of those carbon nanotubes using the π orbital axis vector 1 (POAV1) analysis.[42,43] The π orbital axis makes equal angles with all three σ bonds at the conjugated carbon atom in question. The angle between the π orbital axis vector and the σ bond is 90° for a planar molecule. The pyramidalization angle θ_P is then defined as the deviation of this angle from 90°. The larger θ_P is the larger the rehybridization of the σ and π electrons.[42] For (3,3) and (5,0), we obtain $\theta_P = 9.9°$ and 10.0°, respectively. For (4,2) $C_{220}H_{12}$, θ_P values are 9.6−9.7° depending on the atoms. Since the θ_P values have no clear correlation with the optical gaps, we conjecture that the differences in the optical spectra of (4,2), (3,3), and (5,0) are caused mainly by the relative positions of the carbon atoms.

3.2. Dipole-Allowed Optical Transitions. Armchair and zigzag SWNTs are highly symmetric. Depending on the way

(42) Haddon, R. C. *Acc. Chem. Res.* **1988**, *21*, 243.
(43) Haddon, R. C. *J. Phys. Chem. A* **2001**, *105*, 4164.

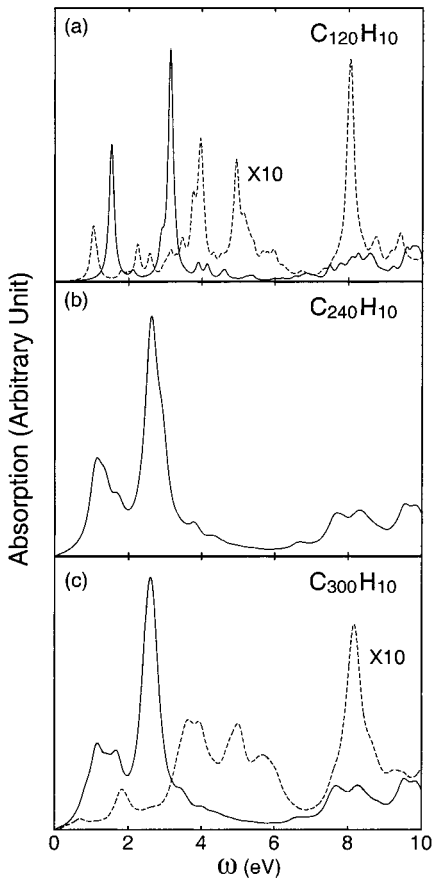

Figure 4. The calculated absorption spectra of zigzag (5,0) SWNTs with dephasing parameter $\gamma = 0.08$ (a) and 0.2 eV in (b and c). The solid lines are the results for the **E** || tube and the dashed lines for the **E** ⊥ tube. The dashed lines are magnified 10 times.

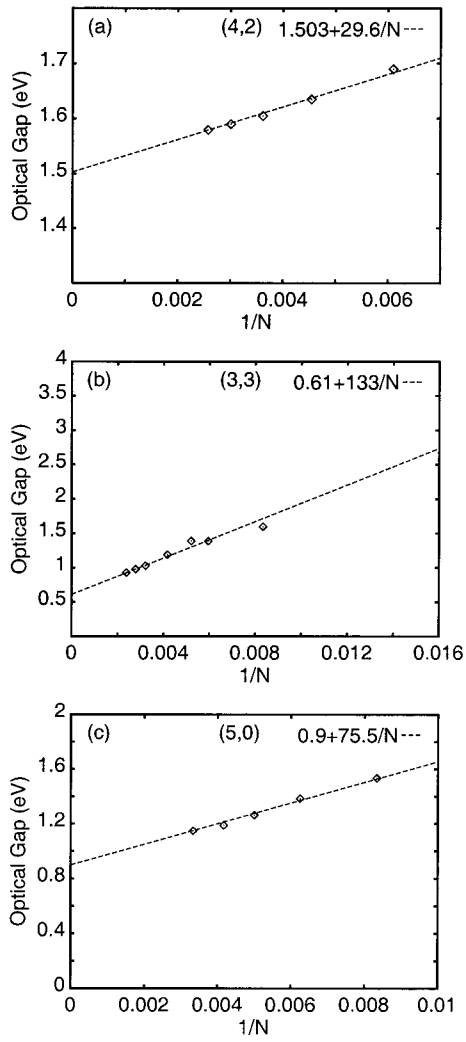

Figure 5. The optical gap versus $1/N$ for open-ended (4,2), (3,3), and (5,0) SWNTs for the **E** || tube, where N is the number of carbon atoms. The dashed lines are linear fits to the calculated results. The optical gaps are 1.50, 0.61, and 0.90 eV for infinite (4,2), (3,3), and (5,0) SWNTs, respectively.

we terminate the open CNTs, (3,3) and (5,0) CNTs may have D_{3h} or D_{3d} and D_{5h} or D_{5d} symmetry, respectively.[41] When the lengths of the (3,3) and (5,0) SWNTs are large enough (>25 Å), the difference in optical response caused by different symmetries can be neglected.[41,44] We examine (3,3) SWNTs with D_{3d} symmetry and (5,0) with D_{5h} here. For the dipole-allowed optical transition, the matrix element $\langle\Phi_i|\mathbf{r}|\Phi_f\rangle$ is nonzero, where **r** is parallel to the electric field **E** and $|\Phi_i\rangle$ ($|\Phi_f\rangle$) is the initial (final) electronic state. D_{3d} has six irreducible representations, A_{1g}, A_{2g}, E_g, A_{1u}, A_{2u}, and E_u. D_{5h} has eight irreducible representations A_1', A_2', E_1', E_2', A_1'', A_2'', E_1'', and E_2''.[45] For the electric field **E** || tube, the following transitions are allowed between the pairs of the molecular orbitals: for (3,3) SWNTs, $A_{1g} \leftrightarrow A_{2u}$, $A_{2g} \leftrightarrow A_{1u}$, and $E_u \leftrightarrow E_g$; for (5,0) SWNTs, $E_1' \leftrightarrow E_1''$, $E_2' \leftrightarrow E_2''$, and $A_1' \leftrightarrow A_2''$. For the electric field **E** ⊥ tube, the allowed transitions are the following: for (3,3), $A_{1g} \leftrightarrow E_u$, $A_{2g} \leftrightarrow E_u$, $A_{1u} \leftrightarrow E_g$, $A_{2u} \leftrightarrow E_g$, and $E_u \leftrightarrow E_g$; for (5,0), $A_1' \leftrightarrow E_1'$, $A_1' \leftrightarrow E_2'$, $A_2' \leftrightarrow E_1'$, $A_2' \leftrightarrow E_2'$, $A_2'' \leftrightarrow E_1''$, $A_2'' \leftrightarrow E_2''$, $A_1'' \leftrightarrow E_1''$, and $A_1'' \leftrightarrow E_2''$. For the open-ended (3,3) SWNTs, the molecular orbitals with A_{1g}, A_{2g}, A_{1u}, and A_{2u} symmetry are found energetically close to the HOMO and LUMO. The molecular orbitals with E_u and E_g symmetry are quite different in energy from HOMO and LUMO. The excitation at 1.57 eV of (3,3) $C_{120}H_{12}$ for the **E** || tube consists mainly of the transition $A_{1g} \leftrightarrow A_{2u}$ and $A_{2a} \leftrightarrow A_{1u}$ while the first excitation for the **E** ⊥ tube consists mainly of $A_{1g} \leftrightarrow E_u$, $A_{1u} \leftrightarrow E_g$, $A_{2g} \leftrightarrow E_u$, and $A_{2u} \leftrightarrow E_g$ transitions. This explains the fact that the optical gap for the **E** ⊥ tube is larger than that for the **E** || tube for (3,3) SWNTs.

The induced density matrices $\delta\rho$ of the transitions corresponding to the absorption peaks at 1.57 and 4.58 eV of (3,3) $C_{120}H_{12}$, 1.53 and 3.14 eV of (5,0) $C_{120}H_{10}$, and 0.61 and 2.49 eV of (4,2) $C_{52}H_{12}$ are obtained. To examine them, we project the induced density matrices onto the HFMO representation.[46] In other words, the dipole-induced excitations are decomposed into the transitions between the pairs of molecular orbitals. The results are shown in Tables 1−3. The molecular orbital transitions whose absolute amplitudes are larger than 0.1 are listed. Since $|\delta\rho_{ij}| = |\delta\rho_{ji}|$, only $\delta\rho_{ij}$ ($i < j$) are shown, where i and j stand for a pair of the molecular orbitals. For (3,3) $C_{120}H_{12}$, the excitation at 1.57 eV is a $\pi^*-\pi$ transition and consists mainly of the HOMO to LUMO+1 and HOMO−1 to LUMO transitions with their respective amplitudes 0.44 and 0.36 (see Table 1). Other contributions, such as the HOMO−2 to LUMO+3 and HOMO−3 to LUMO+2, are much smaller. The excitation at 4.58 eV is also a $\pi-\pi^*$ transition. Its main contributions are from the pairs of molecular orbitals with E_u and E_g symmetry (see Table 1). The transition from HOMO to LUMO is forbidden for (3,3) CNTs, since they have A_{1g} and

(44) Rochefort, A.; Salahub, D. R.; Avouris, P. *J. Phys. Chem. B* **1999**, *103*, 641.

(45) Ludwig, W.; Falter, C. *Symmetries in Physics: group theory applied to physical problems*; Springer: New York, 1996.

(46) Chen, G. H.; Mukamel, S. *J. Am. Chem. Soc.* **1995**, *117*, 4945.

Table 1. The Compositions of the Photoinduced Transitions at 1.57 and 4.58 eV of (3,3) $C_{120}H_{12}$[a]

1.57 eV	
HOMO-1(A_{1u}) → LUMO(A_{2g})	0.36
HOMO(A_{1g}) → LUMO+1(A_{2u})	0.44
HOMO-3(A_{2g}) → LUMO+2(A_{1u})	−0.15
HOMO-2(A_{2u}) → LUMO+3(A_{1g})	−0.19
4.58 eV	
HOMO-18(E_u) → LUMO+9(E_g)	−0.11
HOMO-10(E_u) → LUMO+9(E_g)	0.16
HOMO-9(E_u) → LUMO+9(E_g)	−0.12
HOMO-17(E_u) → LUMO+10(E_g)	−0.11
HOMO-10(E_u) → LUMO+10(E_g)	0.14
HOMO-9(E_u) → LUMO+10(E_g)	0.16
HOMO-11(E_g) → LUMO+11(E_u)	−0.23
HOMO-12(E_g) → LUMO+12(E_u)	0.23
HOMO-13(E_g) → LUMO+13(E_u)	−0.13
HOMO-14(E_g) → LUMO+14(E_u)	0.13
HOMO-15(E_u) → LUMO+15(E_g)	−0.13
HOMO-16(E_u) → LUMO+16(E_g)	0.13

[a] The first column lists the transitions between pairs of molecular orbitals, and the second column lists the corresponding composition coefficients of the specific transitions between the molecular orbital pairs.

Table 2. The Compositions of the Photoinduced Transitions at 1.53 and 3.14 eV of (5,0) $C_{120}H_{10}$[a]

1.53 eV	
HOMO-10(E_1'') → LUMO(E_1')	0.12
HOMO-11(E_1'') → LUMO+1(E_1')	0.12
HOMO-4(E_2') → LUMO+3(E_2'')	0.19
HOMO(E_2') → LUMO+3(E_2'')	−0.28
HOMO-5(E_2') → LUMO+4(E_2'')	0.19
HOMO-1(E_2') → LUMO+4(E''_2)	0.28
HOMO-6(E_2'') → LUMO+8(E_2')	0.10
HOMO-3(E_2'') → LUMO+8(E_2')	0.13
HOMO-2(E_2'') → LUMO+8(E_2')	−0.20
HOMO-7(E_2'') → LUMO+9(E_2')	0.10
HOMO-3(E_2'') → LUMO+9(E_2')	−0.20
HOMO-2(E_2'') → LUMO+9(E'_2)	−0.13
HOMO-1(E_2') → LUMO+13(E_2'')	0.11
HOMO(E_2') → LUMO+13(E_2'')	0.11
HOMO-1(E_2') → LUMO+14(E_2'')	−0.11
HOMO(E_2') → LUMO+14(E_2'')	0.11
3.14 eV	
HOMO-10(E_1'') → LUMO(E_1')	−0.25
HOMO-11(E_1'') → LUMO+1(E_1')	−0.25
HOMO-24(A_2'') → LUMO+2(A_1')	−0.11
HOMO-4(E_2') → LUMO+3(E_2'')	0.19
HOMO(E_2') → LUMO+3(E_2'')	0.12
HOMO-5(E_2') → LUMO+4(E_2'')	0.19
HOMO-1(E'_2) → LUMO+4(E_2'')	−0.12
HOMO-14(E_1') → LUMO+6(E_1'')	0.10
HOMO-15(E_1') → LUMO+7(E_1'')	0.10
HOMO-6(E_2'') → LUMO+8(E_2')	0.11
HOMO-7(E_2'') → LUMO+8(E_2')	0.11

[a] The first column lists the transitions between pairs of molecular orbitals, and the second column lists the corresponding composition coefficients of the specific transitions between the molecular orbital pairs.

A_{2g} symmetry, respectively. For (5,0) $C_{120}H_{10}$, the excitations at 1.53 and 3.14 eV are from $\pi-\pi^*$ transitions. The molecular orbitals involved in the transitions have E_1', E_1'', E_2', and E_2'' symmetry (see Table 2). $A_2'' \leftrightarrow A_1'$ transition has a small contribution to the excitation at 3.14 eV. HOMO to LUMO transition is forbidden for (5,0) as well. For (4,2) $C_{52}H_{12}$, the excitation at 0.61 eV is a $\pi-\pi^*$ transition, and its main contributions are from the HOMO to LUMO, HOMO−1 to LUMO+1, and HOMO−2 to LUMO+4 transitions. The excitation at 2.49 eV is also a π to π^* transition with the HOMO−1 to LUMO+1 transition as the main contribution (see Table 3).

Table 3. The Compositions of the Photoinduced Transitions at 0.61 and 2.49 eV of (4,2) $C_{52}H_{12}$[a]

0.61 eV	
HOMO → LOMO	−0.72
HOMO−1 → LOMO+1	−0.34
HOMO−2 → LOMO+4	−0.25
HOMO−4 → LOMO+6	0.12
2.49 eV	
HOMO → LOMO	−0.15
HOMO−1 → LOMO+1	0.53
HOMO−3 → LOMO+2	0.19
HOMO−5 → LOMO+3	−0.18
HOMO−2 → LOMO+4	0.19
HOMO−4 → LOMO+6	−0.15
HOMO−2 → LOMO+6	0.14

[a] The first column lists the transitions between pairs of molecular orbitals, and the second column lists the corresponding composition coefficients of the specific transitions between the molecular orbital pairs.

3.3. Chirality of 4 Å SWNT. The absorption spectra of the 4 Å SWNTs reported in ref 35 was measured recently.[36] The polarization of the light was tuned to examine the anisotropy of the optical response. Several important observations were obtained. (1) For the **E** || tube, three absorption peaks were identified at 1.35, 2.15, and 3.10 eV. (2) As **E** deviates from the tube's parallel direction to its normal direction, the absorption intensity weakens significantly, and moreover, the spectra red shift. (3) The 4 Å SWNTs are transparent for the **E** ⊥ tube. The (4,2) SWNT has been ruled out because it costs much energy to fit the half C_{20} cap.[33,35] In addition, its calculated absorption spectra do not agree with the experimental results.[36] The 4 Å SWNTs may be either (3,3) or (5,0) because they fit well with the half of C_{20} cap.[33,35] Examining the absorption spectra of (3,3) SWNTs, we rule out the (3,3) SWNT. This is because (i) the (3,3) has one major absorption peak below 4.0 eV and locates at a very low energy of 0.61 eV for the infinitely long tube and (ii) the optical gap for the **E** ⊥ tube is larger than the optical gap for the **E** || tube, which is contradictory to the experimental observation that the absorption spectra red shift as the light polarization deviates from the tube axis. On the contrary, the calculated absorption spectra of (5,0) are in reasonable agreement with the experimental absorption spectra. For the **E** || tube, there are three absorption peaks below 4 eV. This agrees qualitatively with the measured absorption spectra for 4 Å SWNTs. Admittedly, the calculated spectra red shift with respect to the experimental absorption spectra. This is due to the PM3 Hamiltonian that was not optimized for the time-dependent Hartree−Fock (TDHF) method used in the LDM method.[27−30] For the **E** ⊥ tube, the first absorption peak red shifts to 0.7 eV from 1.16 eV for the **E** || tube, see Figure 4c, which agrees with the observed red shift of the absorption spectra due to the light polarization. Therefore, we conclude that 4 Å SWNTs synthesized in the channels of porous zeolite $ALPO_4$-5 (AFI) single crystals[35] are the (5,0) SWNTs.

4. Conclusion

The absorption spectra and electronic structures of 4 Å single-walled (4,2), (3,3), and (5,0) SWNTs are calculated by the LDM-PM3 method. A qualitative picture has emerged regarding the optical transitions in these small SWNTs. The main conclusions are summarized as follows.

(1) Distinctive absorption spectra are found for (4,2), (3,3), and (5,0) SWNTs. The chirality has a strong influence on the absorption spectra of 4 Å SWNTs. This differs from the previous findings[30] of the larger diameter SWNTs where the chirality

has much less effect on the absorption spectra. This is reaffirmed by our calculations on the two larger SWNTs, the (9,0) C_{294} and the (5,5) C_{290}.

(2) Because of the sensitive effects of the chirality, the absorption spectra are used to determine the structure of 4 Å SWNT. By comparing the measured and calculated absorption spectra, we conclude that the 4 Å SWNTs reported in ref 35 are the (5,0) SWNTs.

(3) The optical responses of the 4 Å SWNTs are highly anisotropic. This is because that the transition dipole moments parallel to the tube are much larger than the moments perpendicular to the tube. The anisotropy is clearly demonstrated in Figures 2−4.

(4) Similar to the findings of the larger diameter SWNTs, the optical gaps of the infinite (3,3), (4,2), and (5,0) SWNTs are all finite, being 0.6, 1.5, and 0.9 eV, respectively. This is despite the fact that the LDA calculation predicts that all three 4 Å SWNTs are metallic.[26] The existence of the finite optical gap is consistent with the measured absorption spectra.[36]

Acknowledgment. Support from the Hong Kong Research Grant Council (RGC) and the Committee for Research and Conference Grants (CRCG) of the University of Hong Kong is gratefully acknowledged.

Supporting Information Available: Absorption spectra of the single-walled 4 Å carbon nanotubes for different polarizations (PDF). This material is available free of charge via the Internet at http://pubs.acs.org.

JA0160445